ISSN (Print) 1226-1750
ISSN (Online) 2233-6656
Journal of Magnetics 25(4), 577-583 (2020) https://doi.org/10.4283/JMAG.2020.25.4.577

Comparative Investigation of Ferromagnetic Hybrid Nanomaterials (Nickle Zinc Ferrite, Manganese Zinc Ferrite) in Darcy-Forchheimer Flow with Wu's Slip

Yu-Ming Chu[1,2], M. Ijaz Khan[3]*, F. Alzahrani[4], and A. Hobiny[4]

[1]*Department of Mathematics, Huzhou University, Huzhou 313000, PR China*
[2]*Hunan Provincial Key Laboratory of Mathematical Modeling and Analysis in Engineering, Changsha University of Science & Technology, Changsha 410114, PR China*
[3]*Department of Mathematics and Statistics, Riphah International University I-14, Islamabad 44000, Pakistan*
[4]*Nonlinear Analysis and Applied Mathematics (NAAM)-Research Group, Department of Mathematics, Faculty of Sciences, King Abdulaziz University, P.O. Box 80203, Jeddah 21589, Saudi Arabia*

(Received 3 October 2020, Received in final form 19 December 2020, Accepted 22 December 2020)

Abstract: This paper study the hybrid nanofluid flow over a stretching sheet with additional effect of Wu's slip. Comparative study of four different hybrid nanofluids is done here. We have considered manganese zinc ferrite $NnZnFe_2O_4$, Nickle zinc ferrite $NiZnFe_2O_4$ as nanoparticles whereas Kerosene oil $C_{10}H_{22}$ and Engine oil C_8H_{18} as base fluids. Darcy Forchheimer porous medium is considered in momentum equation. Heat equation is studied in presence of different effects namely radiation, convective condition, temperature dependent heat source sink and viscous dissipation. Transformations are applied on PDE's to form the governing equation of ODE's. Shooting method technique is used to solve the governing equations. Velocity, temperature, Nusselt number and skin friction behaviour against different parameters is analyzed via graphs. Velocity of the fluid decays for higher slip parameter. Motion of the fluid increases for greater values of Forchheimer number. Temperature is increasing function of Biot number.

Keywords : Wu's slip, hybrid nanofluid, darcy forchheimer, radiation, convective condition, temperature dependent heat source sink, viscous dissipation

1. Introduction

Nanofluid in past decade gain so much interest of researchers and engineers in different areas of technology. The purpose of nanofluid is to enhance the base fluid's convective heat transfer and thermal performance by adding nanoparticles in it. Initially Choi [1] was the one who worked on nanofluid. These type of liquids are formed by adding nanoparticles of size (< 100 nm) in to base liquids like water, kerosene oil, engine oil etc. Nanoparticles are used to change the thermal characteristics of base fluid. Heat transport characteristics are enhanced due to addition of these nanoparticles with high rate of thermal conductivity. Nowadays a new terminology is used for nanofluid is hybrid nanofluid. In these type of fluids more than two nanoparticles or more than two base fluids are mixed to make a nanofluid. These type of fluids are more affected than simple nanofluid. Lin *et al.* [2] scrutinized the non-Newtonian nanofluid flow over a thin finite film with heat source effect. Madhu *et al.* [3] presented the flow of nanofluid by considering four different nanoparticles with power law viscosity effect. Maxwell nanofluid flow with stagnation point is studied by Bai *et al.* [4]. Ethylene glycol-titanium dioxide nanofluid with heat source sink is studied by Hosseinzadeh *et al.* [5]. Maxwell nanofluid flow over a convectively heated surface is elaborated by Jusoh *et al.* [6]. Nanofluid flow with gyrotactic microorganism considering convective conditions is studied by Xu and Pop [7]. Williamson nanofluid bidirectional flow with extra effect of mixed convection is studied by Hayat *et al.* [8]. Tangent hyperbolic nanofluid radiative flow with activation energy is delineated by Ijaz *et al.* [9]. Sisko nanofluid flow between two stretchable disks is explained by Ijaz *et al.* [10].

*Corresponding author: Tel: +92-335-9761475
Fax: +92-335-9761475, e-mail: mikhan@math.qau.edu.pk

Some more studies regarding nanofluid and hybrid nanofluid can be seen through Refs. [11-20].

Purpose of this paper is to study hybrid nanofluid flow over a stretching sheet with additional effect of Wu's slip. Comparative study of four different hybrid nanofluids is done here. We have considered manganese zinc ferrite $MnZnFe_2O_4$, Nickle zinc ferrite $NiZnFe_2O_4$ as nanoparticles whereas Kerosene oil $C_{10}H_{22}$ and Engine oil C_8H_{18} as base fluids. Some more important effects are studied in this paper namely Darcy Forchheimer porous medium, temperature dependent heat source sink, radiation, convective condition and viscous dissipation. Built in Shooting method is used to find the solution of the problem. Characteristics of fluid are elaborated through graphs.

2. Mathematical Formulation

Here we have study the flow of different hybrid nanofluids by stretching sheet. Wu's slip condition is used for momentum equation. Darcy forchheimer porous medium is used in a momentum equation. Thermal equation is formed by considering the effect of radiation, convective condition, Temperature dependent heat source sink and viscous dissipation. Zinc ferrite $MnZnFe_2O_4$ and Nickle Zinc ferrite $NiZnFe_2O_4$ are used as nanoparticles and Kerosene oil and engine oil are used as base fluids. According to above assumptions flow equations are formed as below:

$$\frac{\partial u}{\partial x} + \frac{\partial v}{\partial y} = 0\,, \tag{1}$$

$$\rho_{hnf}\left(u\frac{\partial u}{\partial x} + v\frac{\partial u}{\partial y}\right) = -\frac{\partial p}{\partial x} + \mu_{hnf}\frac{\partial^2 u}{\partial y^2} - \frac{\mu_{hnf}}{K^0}u - Fu^2\,, \tag{2}$$

$$(\rho C_p)_{hnf}\left(u\frac{\partial u}{\partial x} + v\frac{\partial u}{\partial y}\right) = k_{hnf}\frac{\partial^2 T}{\partial y^2} + \frac{16\sigma^* T_\infty^3}{3k^*}\frac{\partial^2 T}{\partial y^2} + \mu_{hnf}\left(\frac{\partial u}{\partial y}\right)^2$$
$$+ Q_0(T_f - T_\infty)\exp(-nv^{-0.5}\Omega^{0.5}y) + Q_l(T - T_\infty)\,, \tag{3}$$

Boundary conditions

$$u = ax + U_{Wu's\ slip},\ v = 0,\ k_{hnf}\frac{\partial T}{\partial y} = -h_1(T_f - T)\,,$$
$$u \to 0,\ T \to T_\infty\,, \tag{4}$$

$$U_{slip} = A\frac{\partial u}{\partial y} + B\frac{\partial^2 u}{\partial y^2}\,, \tag{5}$$

where (u, v) are velocity vector, (x, y) are Cartesian coordinates, ρ_{hnf}, μ_{hnf}, K^0, $F = \frac{C_b}{xK^{0\,1/2}}$, $(\rho C_p)_{hnf}$, k_{hnf}, Q_0, k^*, σ^*, n, T, Q_l, A, B, and h_1 are known as density of hybrid nanofluid, dynamic viscosity of hybrid nanofluid, porosity constant, Forchheimer coefficient, heat capacitance of hybrid nanofluid, thermal conductivity of hybrid nanofluid, thermal dependent heat coefficient, mean absorption coefficient, exponential index, Temperature of fluid, exponential dependent heat source, first order velocity slip, second order velocity slip and heat transfer coefficient.

Similarity transformations

$$\xi = y\sqrt{\frac{a}{v_f}},\ u = axf'(\xi),\ v = -\sqrt{a\,v_f}f(\xi),\ \theta(\xi) = \frac{T - T_\infty}{T_f - T_\infty} \tag{6}$$

where $v_f = v_{f1} + v_{f2}$ in case of two base fluid.

Dimensionless form

$$\frac{f'''}{(1-\phi_1)^{5/2}(1-\phi_2)^{5/2}A_1} + ff'' - f'^2$$
$$- \frac{f'}{K^*(1-\phi_1)^{5/2}(1-\phi_2)^{5/2}A_1} - F_r f'^2 = 0 \tag{7}$$

$$\frac{1}{PrA_2}\left[\frac{k_{hnf}}{k_{f1}+k_{f2}} + R\right]\theta'' + f\theta' + \frac{Q_e}{A_2}\exp(-n\xi)$$
$$+ \frac{Q_t}{A_2}\theta + \frac{f''^2}{(1-\phi_1)^{5/2}(1-\phi_2)^{5/2}A_2} = 0\,, \tag{8}$$

Corresponding reduced boundary conditions

$$f'(0) = 1 + L_1 f''(0) + L_2 f'''(0),\ f(0) = 0\,,$$
$$\theta'(0)\frac{k_{hnf}}{k_{f1}+k_{f2}} = -B_1(1-\theta(0))$$
$$f'(\infty) \to 0,\ \theta(\infty) \to 0 \tag{9}$$

Where R is radiation parameter, Pr is Prandtl number, L_1 is slip parameter, L_2 second order slip parameter, B_1 is Biot number, K^* is porosity parameter, F_r is Forchheimer number, Q_t is thermal dependent heat source parameter, Q_e exponential dependent heat source parameter.

$$R = \frac{16\sigma^* T_\infty^3}{3k^*(k_{f1}+k_{f2})},\ Pr = \frac{((\rho C_p)_{f1} + (\rho C_p)_{f2})\,v_f}{k_{f1}+k_{f2}},$$
$$L_1 = A\sqrt{\frac{a}{v}},\ L_2 = B\frac{a}{v_f},\ B_1 = \frac{h_1}{k_{f1}+k_{f2}}\sqrt{\frac{v_f}{a}}$$
$$A_1 = \frac{\rho_{hnf}}{(\rho_{f1}+\rho_{f2})},\ A_2 = \frac{(\rho Cp)_{hnf}}{(\rho Cp)_{f1} + (\rho Cp)_{f2}},\ K^* = \frac{v_f}{K^0 a},$$
$$F_r = \frac{C_b}{K_0^{0.5}},\ Q_t = \frac{Q_l}{((\rho Cp)_{f1} + (\rho Cp)_{f2})a},$$
$$Q_e = \frac{Q_0}{((\rho Cp)_{f1} + (\rho Cp)_{f2})a}\,. \tag{10}$$

Skin friction and Nusselt number in dimensional form is

$$C_{fx} = \frac{\tau_w}{(\rho_{f1} + \rho_{f2})U_w^2},\ Nu_x = \frac{xq_w}{(k_{f1} + k_{f2})(T_w - T_\infty)} \qquad (11)$$

Where

$$\tau_w = (\mu_{f1} + \mu_{f2})\frac{\partial u}{\partial y},\ q_w = -k_{hnf}\frac{\partial T}{\partial y} - \frac{16\sigma^* T_\infty^3}{3k^*}\frac{\partial T}{\partial y} \qquad (12)$$

In dimensional form

$$Re^{0.5}C_{fx} = \frac{1}{(1-\phi_1)^{5/2}(1-\phi_2)^{5/2}}f''(0),\ Nu_x Re^{-0.5} = -\left(\frac{k_{hnf}}{k_{f1} + k_{f2}} + R\right)\theta'(0). \qquad (13)$$

Table 1. Thermo physical properties of base fluid and ferrite nanoparticles.

Physical properties	ρ (kg/m^3)	C_p (J/kgK)	k (W/mK)	Pr
$C_{10}H_{22}$	783	2090	0.15	21
C_8H_{18}	890	1868	0.145	12900
$NiZnFe_2O_4$	4800	710	6.3	-
$MnZnFe_2O_4$	4700	1050	3.9	-

Table 2. Thermo physical properties of $MnZnFe_2O_4 - NiZnFe_2O_4 - C_{10}H_{22}$ and $MnZnFe_2O_4 - NiZnFe_2O_4 - C_{10}H_{22} - C_8H_{18}$.

Properties	$MnZnFe_2O_4 - NiZnFe_2O_4 - C_{10}H_{22}$	$MnZnFe_2O_4 - NiZnFe_2O_4 - C_{10}H_{22} - C_8H_{18}$
Density (ρ)	$\frac{\rho_{hnf}}{\rho_f}(1-\phi_2)\left[(1-\phi_1) + \phi_1\frac{\rho_{S1}}{\rho_f}\right] + \phi_2\frac{\rho_{S2}}{\rho_f}$	$\frac{\rho_{hnf}}{(\rho_{f1}+\rho_{f2})}(1-\phi_2)\left[(1-\phi_1) + \phi_1\frac{(\rho_{S1}+\rho_{S2})}{(\rho_{f1}+\rho_{f2})}\right] + \phi_2\frac{(\rho_{S1}+\rho_{S2})}{(\rho_{f1}+\rho_{f2})}$
Heat capacity (ρC_p)	$\frac{(\rho Cp)_{hnf}}{(C_p\rho)_f} = (1-\phi_1)\left[(1-\phi_1) + \phi_1\frac{(\rho Cp)_{S1}}{(\rho Cp)_f}\right] + \phi_2\frac{(\rho Cp)_{S2}}{(\rho Cp)_f}$	$\frac{(\rho Cp)_{hnf}}{(\rho Cp)_{f1} + (\rho Cp)_{f2}} = (1-\phi_2)\left[(1-\phi_1) + \phi_1\frac{(\rho Cp)_{S1} + (\rho Cp)_{S2}}{(\rho Cp)_{f1} + (\rho Cp)_{f2}}\right] + \phi_2\frac{(\rho Cp)_{S1} + (\rho Cp)_{S2}}{(\rho Cp)_{f1} + (\rho Cp)_{f2}}$
Viscosity (μ)	$\mu_{hnf} = \frac{\mu_f}{(1-\phi_1)^{2.5}(1-\phi_2)^{2.5}}$	$\mu_{hnf} = \frac{\mu_{f_1} + \mu_{f_2}}{(1-\phi_1)^{2.5}(1-\phi_2)^{2.5}}$
Thermal conductivity	$\frac{k_{hnf}}{k_{bf}} = \frac{k_{S_2} + 2k_{bf} - 2\phi_2(k_{bf} - k_{S_2})}{k_{S_2} + 2k_{bf} + \phi_2(k_{bf} - k_{S_2})}$, $\frac{k_{bf}}{k_f} = \frac{k_{S_1} + 2k_f - 2\phi_1(k_f - k_{S_1})}{k_{S_1} + 2k_f + \phi_1(k_f - k_{S_1})}$,	$\frac{k_{hnf}}{(k_{bf_1} + k_{bf_1})} = \frac{(k_{S_1} + k_{S_2}) + 2(k_{bf_1} + k_{bf_1}) - 2\phi_2((k_{bf_1} + k_{bf_1}) - (k_{S_1} + k_{S_2}))}{(k_{S_1} + k_{S_2}) + 2(k_{bf_1} + k_{bf_1}) + \phi_2(k_{bf} + (k_{S_1} + k_{S_2}))}$ $\frac{(k_{bf_1} + k_{bf_1})}{(k_{f_1} + k_{f_1})} = \frac{(k_{S_1} + k_{S_2}) + 2(k_{f_1} + k_{f_1}) - 2\phi_2((k_{f_1} + k_{f_1}) - (k_{S_1} + k_{S_2}))}{(k_{S_1} + k_{S_2}) + 2(k_{f_1} + k_{f_1}) + \phi_1((k_{f_1} + k_{f_1}) - (k_{S_1} + k_{S_2}))}$,
Prandtl number	21	12921

Table 3. Thermo physical properties of $MnZnFe_2O_4 - C_{10}H_{22}$ and $MnZnFe_2O_4 - NiZnFe_2O_4 - C_8H_{18}$.

Properties	$MnZnFe_2O_4 - C_{10}H_{22}$	$MnZnFe_2O_4 - NiZnFe_2O_4 - C_8H_{18}$
Density (ρ)	$\rho_{nf} = (1-\phi)\rho_f + \phi\rho_s$	$\frac{\rho_{hnf}}{\rho_f} = (1-\phi_2)\left[(1-\phi_1) + \phi_1\frac{\rho_{S1}}{\rho_f}\right] + \phi_2\frac{\rho_{S2}}{\rho_f}$
Heat capacity (ρC_p)	$(\rho Cp)_{nf} = (1-\phi_1)(\rho C_p)_f + \phi(\rho C_p)_s$	$\frac{(\rho Cp)_{hnf}}{(C_p\rho)_f} = (1-\phi_2)\left[(1-\phi_1) + \phi_1\frac{(\rho Cp)_{S1}}{(\rho Cp)_f}\right] + \phi_2\frac{(\rho Cp)_{S2}}{(\rho Cp)_f}$
Viscosity (μ)	$\mu_{nf} = \frac{\mu_f}{(1-\phi_1)^{2.5}}$	$\mu_{hnf} = \frac{\mu_f}{(1-\phi_1)^{2.5}(1-\phi_2)^{2.5}}$
Thermal conductivity	$\frac{k_{nf}}{k_f} = \frac{k_S + (n-1)k_f + (n-1)\phi(k_S - k_f)}{k_S + (n-1)k_f + \phi(k_S - k_f)}$	$\frac{k_{hnf}}{k_{bf}} = \frac{k_{S_2} + 2k_{bf_1} - 2\phi_2(k_{bf} - k_{S_2})}{k_{S_2} + 2k_{bf_1} + \phi_2(k_{bf} - k_{S_2})}$, $\frac{k_{bf}}{k_f} = \frac{k_{S_1} + 2k_{f_1} - 2\phi_1(k_f - k_{S_1})}{k_{S_1} + 2k_{f_1} + \phi_1(k_f - k_{S_1})}$
Prandtl number	21	12900

3. Results and Discussion

This section is devoted for physical results of velocity, temperature, Nusselt number, skin friction via different parameters (See Figs. (1-13)). This whole section is devoted for examination of different hybrid nanofluids over a boundary value problem. In this segment Nickle zinc ferrite ($NiZnFe_2O_4$) and maganese zinc ferrite ($MnZnFe_2O_4$) are used as nanoparticles and kerosene oil ($C_{10}H_{22}$) and engine oils (C_8H_{18}) are used as base fluids. Thermophysical values of nanoparticles and base fluids are presented in Table 1. Table 2 and Table 3 are design to show the physical properties of four different hybrid nanofluids.

3.1. Velocity distribution

This subsection is designed for the behaviour of velocity field against different parameters in Figs. (1-6). Fig. 1 shows the trends of four hybrid nanofluids namely $MnZnFe_2O_4 - NiZnFe_2O_4 - C_{10}H_{22} - C_8H_{18}$ hybrid nanofluid, $MnZnFe_2O_4 - NiZnFe_2O_4 - C_{10}H_{22}$ hybrid nanofluid, $MnZnFe_2O_4 - NiZnFe_2O_4 - C_8H_{18}$ hybrid nanofluid and $NiZnFe_2O_4 - C_{10}H_{22}$ nanofluid. It is seen that velocity for $NiZnFe_2O_4 - C_{10}H_{22}$ nanofluid is higher than other hybrid nanofluid. It is due to the fact that in hybrid nanofluids there are two nanoparticles due to which there is more resistance for flow of fluid particles. Fig. 2 displays the effect of second order velocity slip parameter against $MnZnFe_2O_4 - NiZnFe_2O_4 - C_{10}H_{22} - C_8H_{18}$ hybrid nanofluid and $MnZnFe_2O_4 - NiZnFe_2O_4 - C_{10}H_{22}$ hybrid nanofluid. It is seen that overall behaviour of fluid is decreasing but velocity is more in case of $MnZnFe_2O_4 - NiZnFe_2O_4 - C_{10}H_{22}$ hybrid nanofluid. Fig. 3 is for behaviour of second order velocity slip against $NiZnFe_2O_4 - C_{10}H_{22}$ nanofluid. It is seen that velocity for $NiZnFe_2O_4 - C_{10}H_{22}$ nanofluid. Trends show that it is decreasing for both nanofluid but decrease is more for $MnZnFe_2O_4 - NiZnFe_2O_4 - C_{10}H_{22}$ hybrid nanofluid. For impact of slip parameter against $MnZnFe_2O_4 - NiZnFe_2O_4 - C_{10}H_{22}$ hybrid nanofluid and $MnZnFe_2O_4 - NiZnFe_2O_4 - C_{10}H_{22} - C_8H_{18}$ hybrid nanofluid. Velocity reduces for higher values of L_1. Fig. 5 is sketched to show the impact of first order velocity slip against $MnZnFe_2O_4 - NiZnFe_2O_4 - C_{10}H_{22}$ hybrid nanofluid and $NiZnFe_2O_4 - C_{10}H_{22}$ nanofluid. It is seen that velocity decays due to increase in slip

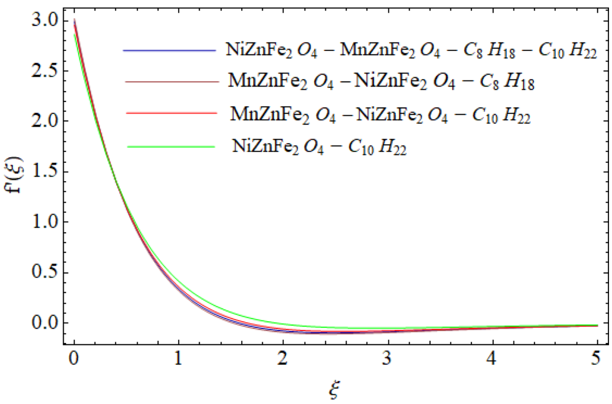

Fig. 1. (Color online) Curve of $f'(\xi)$.

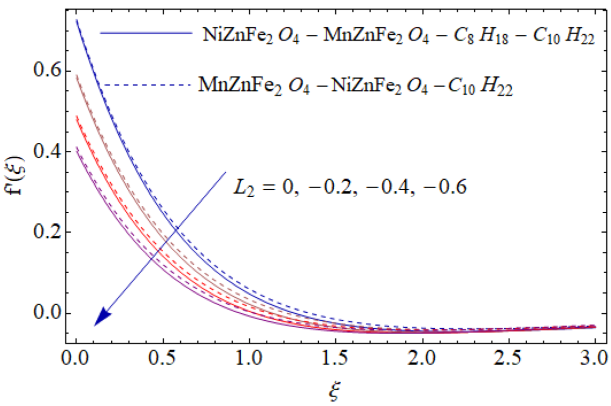

Fig. 2. (Color online) Effect of L_2 on $f'(\xi)$.

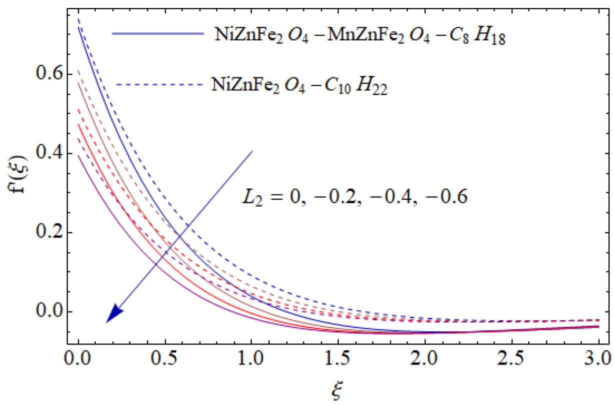

Fig. 3. (Color online) Effect of L_2 on $f'(\xi)$ for two different condition.

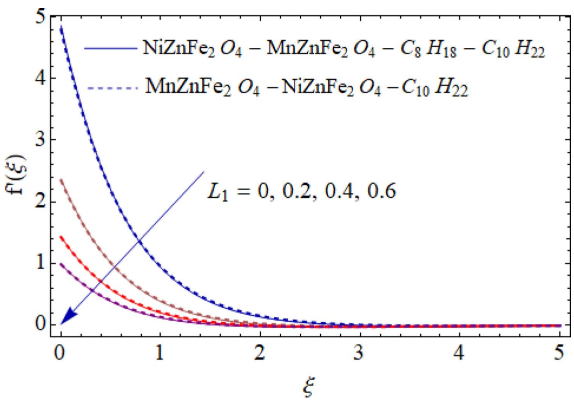

Fig. 4. (Color online) Effect of L_1 on $f'(\xi)$.

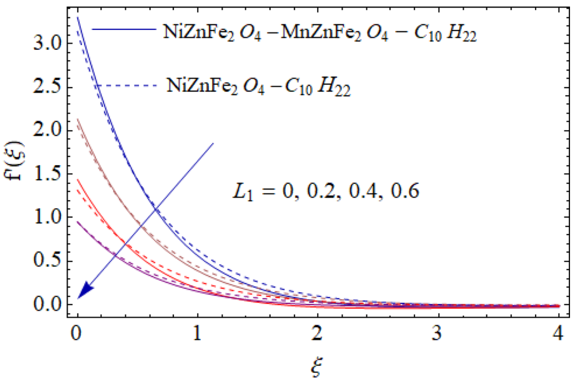

Fig. 5. (Color online) Impact of the L_1 on $f'(\xi)$ with two different hybrid nanofluids.

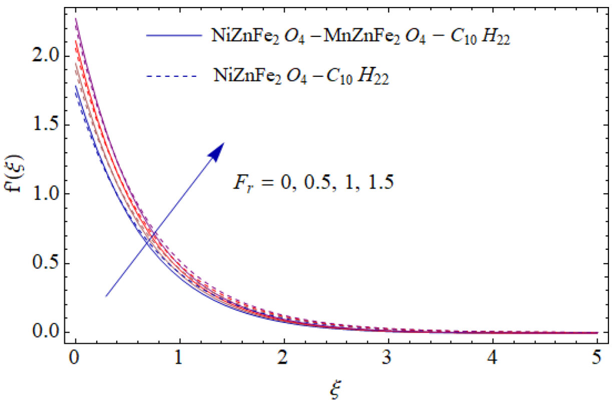

Fig. 6. (Color online) F_r on $f'(\xi)$.

parameter. As we increase the values of slip parameter stretching velocity partially transferred to the fluid due to which velocity decays. Fig. 6 is scrutinized to show the impact of Forchheimer number against $MnZnFe_2O_4$ – $NiZnFe_2O_4$ – $C_{10}H_{22}$ hybrid nanofluid and $NiZnFe_2O_4$ – $C_{10}H_{22}$ nanofluid. It is seen that velocity enhances for greater F_r. It is due to the fact that when we increase the values of porosity constant decays due to which resistance between the fluid particles decays hence velocity increases.

3.2. Thermal distribution

Figs. (7-11) sketched the impact of pertinent parameters against temperature field with different hybrid nanofluids. Fig. 7 tells impact of these four hybrid nanofluid namely $MnZnFe_2O_4$ – $NiZnFe_2O_4$ – $C_{10}H_{22}$ – C_8H_{18} hybrid nanofluid, $MnZnFe_2O_4$ – $NiZnFe_2O_4$ – $C_{10}H_{22}$ hybrid nanofluid, $MnZnFe_2O_4$ – $NiZnFe_2O_4$ – C_8H_{18} hybrid nanofluid and $NiZnFe_2O_4$ – $C_{10}H_{22}$ nanofluid against temperature fluid. It is seen that temperature is highest for $NiZnFe_2O_4$ – $C_{10}H_{22}$ nanofluid. Fig. 8 shows the influence of Biot number via temperature field of $MnZnFe_2O_4$ – $NiZnFe_2O_4$ – $C_{10}H_{22}$ – C_8H_{18} hybrid nanofluid, $MnZnFe_2O_4$ – $NiZnFe_2O_4$ – $C_{10}H_{22}$ hybrid nanofluid. It is seen that temperature

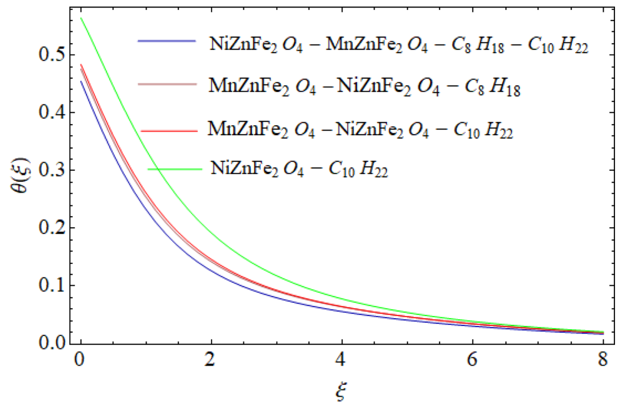

Fig. 7. (Color online) Curves of $\theta(\xi)$ for different hybrid nanofluids.

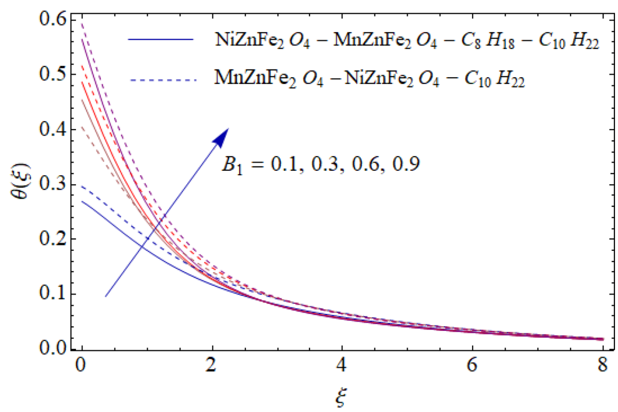

Fig. 8. (Color online) Curve of $\theta(\xi)$ for diverse values of B_1.

rises for greater Biot number due to increase in heat transfer coefficient. It is also observed that $MnZnFe_2O_4$ – $NiZnFe_2O_4$ – $C_{10}H_{22}$ hybrid nanofluid temperature is prominent than other hybrid nanofluid. Impact of thermal heat source parameter via temperature of $MnZnFe_2O_4$ – $NiZnFe_2O_4$ – C_8H_{18} hybrid nanofluid and $NiZnFe_2O_4$ – $C_{10}H_{22}$ nanofluid is presented in Fig. 9. Temperature rises for greater values of Q_t. Physically with increase in Q_t

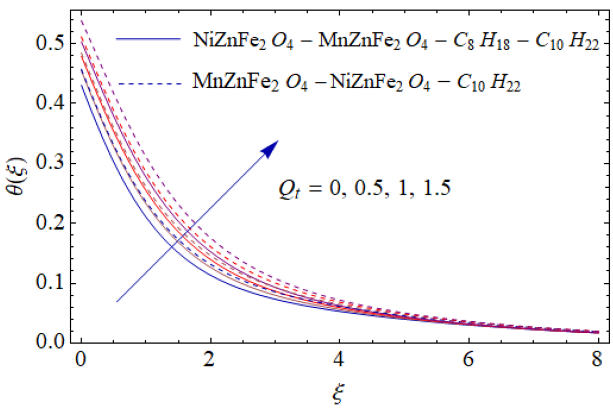

Fig. 9. (Color online) Curve of $\theta(\xi)$ for diverse values of Q_t.

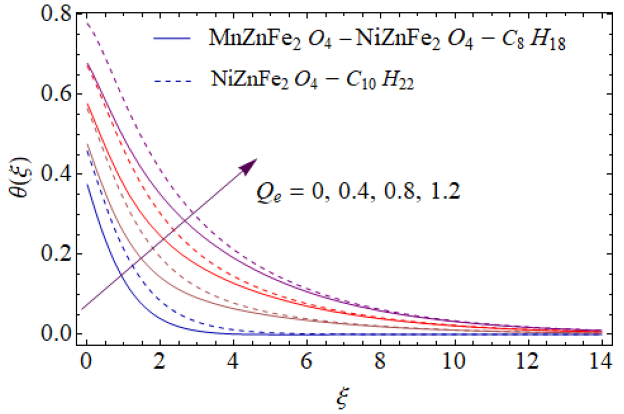

Fig. 10. (Color online) Curve of $\theta(\xi)$ for diverse values of Q_e.

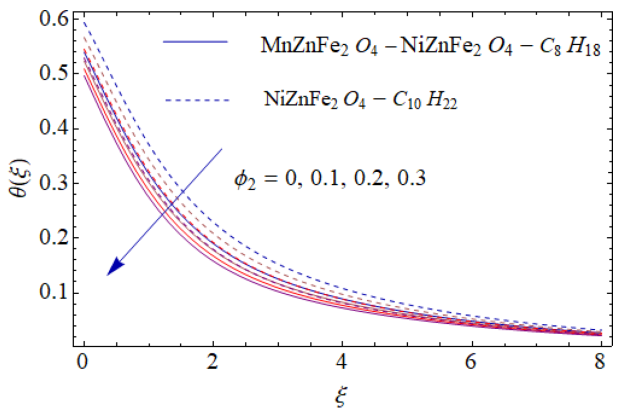

Fig. 11. (Color online) Curve of $\theta(\xi)$ for diverse values of ϕ_2.

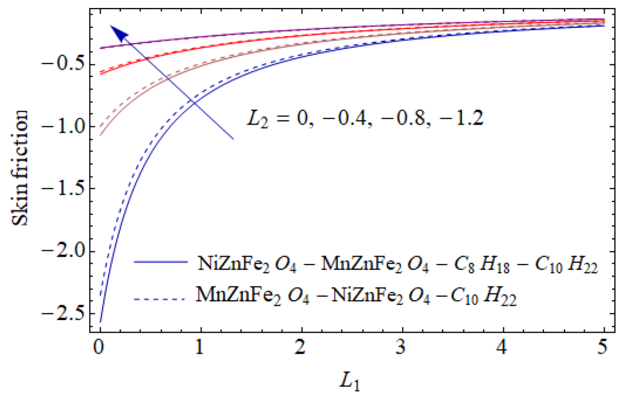

Fig. 12. (Color online) Curve of coefficient of skin friction over L_2.

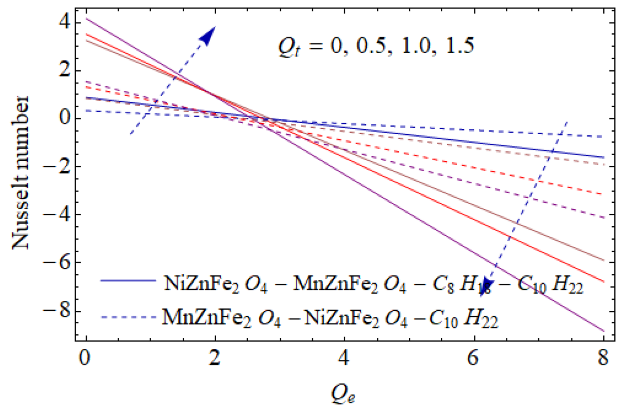

Fig. 13. (Color online) Curve of Nusselt number versus Q_t.

thermal heat source coefficient increases due to which temperature enhances. Fig. 10 shows the impact of temperature field of $MnZnFe_2O_4 - NiZnFe_2O_4 - C_8H_{18}$ hybrid nanofluid and $NiZnFe_2O_4 - C_{10}H_{22}$ nanofluid against exponential heat source parameter Q_e. It is clearly seen that temperature is more for higher values of Q_e. Fig. 11 portrays the impact of nanoparticle volume fraction of $C_{10}H_{22}$ via temperature profile of $MnZnFe_2O_4 - NiZnFe_2O_4 - C_8H_{18}$ hybrid nanofluid and $NiZnFe_2O_4 - C_{10}H_{22}$ nanofluid. It is seen that temperature of the fluid reduces via higher ϕ_2.

3.3. Coefficient of skin friction and rate of heat transfer

Figs. 12 and 13 are designed to show the behaviour of Nusselt number and skin friction against pertinent parameters. Fig. 12 describes that magnitude of surface drag force reduces for higher values of second and first order velocity slip parameters. Fig. 13 tells the influence of thermal heat source parameter against Nusselt number of $MnZnFe_2O_4 - NiZnFe_2O_4 - C_{10}H_{22} - C_8H_{18}$ hybrid nanofluid, $MnZnFe_2O_4 - NiZnFe_2O_4 - C_{10}H_{22}$ hybrid nanofluid. It is observed that Magnitude of Nusselt number boosts up for rising Q_t.

4. Conclusion

Key points of the present analysis are mentioned below:

- Velocity and temperature of $MnZnFe_2O_4 - C_{10}H_{22}$ is more than other nanofluids.
- Velocity of the fluid reduces for higher first and second order velocity slip.
- Temperature enhances for greater values of Q_t and Q_e.
- Temperature of the fluid reduces for greater estimation of ϕ_2.
- Skin friction reduces for higher L_1 and L_2
- Nusselt number is rising for higher Q_t.

Acknowledgments

The research was supported by the National Natural Science Foundation of China (Grant Nos. 11971142, 11871202, 61673169, 11701176, 11626101, 11601485).

References

[1] S. U. S. Choi, Enhancing thermal conductivity of fluids with nanoparticles. ASME-Publicat. Fed, **231**, 99 (1995).

[2] Y. Lin, L. Zheng, X. Zhang, L. Ma, and G. Chen, International Journal of Heat and Mass Transfer **84**, 903 (2015).

[3] M. Madhu, N. Kishan, and A. J. Chamkha, Propulsion and Power Research **6**, 31 (2017).

[4] Y. Bai, X. Liu, Y. Zhang, and M. Zhang, Journal of Molecular Liquids **224**, 1172 (2016).

[5] Hosseinzadeh, K. F. Afsharpanah, S. Zamani, M. Gholinia, and D. D. Ganji, Case Studies in Thermal Engineering **12**, 228 (2018).

[6] R. Jusoh, R. Nazar, and I. Pop, International Journal of Mechanical Sciences **124**, 166 (2018).

[7] H. Xu and I. Pop, International Journal of Heat and Mass Transfer **75**, 610 (2014).

[8] T. Hayat, M. Z. Kiyani, A. Alsaedi, M. I. Khan, and I. Ahmad, International Journal of Heat and Mass Transfer **127**, 422 (2018).

[9] M. I. Khan, S. Qayyum, T. Hayat, M. I. Khan, and T. A. Khan, Physics Letters A **382**, 2017 (2018).

[10] M. I. Khan, T. Hayat, S. Qayyum, M. I. Khan, and A. Alsaedi, Physics Letters A **382**, 2343 (2018).

[11] Y. Zhang and L. Zheng, Chemical Engineering Science **69**, 449 (2012).

[12] M. I. Khan, S. U. Khan, M. Jameel, Y. M. Chu, I. Tlili, and S. Kadry, Surf. Interf. **22**, 100849 (2021).

[13] N. Muhammad and S. Nadeem, Eur. Phys. J. Plus. **132**, 377 (2017).

[14] J. Yang, Z. Abdelmalek, N. Muhammad, and M. T. Mustafa, Int. Commun. Heat Mass Transf. **118**, 104883 (2020), doi: 10.1016/j.icheatmasstransfer.2020.104883.

[15] K. G. Kumar, E. H. B. Hani, M. E. H. Assad, M. Rahimi-Gorji, and S. Nadeem, Microsyst. Technol., Jun. 2020, doi: 10.1007/s00542-020-04920-8.

[16] T. Gul et al., Sci. Rep. **10**, 8474, Dec. 2020, doi: 10.1038/s41598-020-65298-1.

[17] S. Farooq, M. Ijaz Khan, M. Waqas, T. Hayat, and A. Alsaedi, Comput. Methods Programs Biomed. **184**, 105086 (2020), doi: 10.1016/j.cmpb.2019.105086.

[18] V. Vinita and V. Poply, Mater. Today Proc. **26**, 3429 (2020).

[19] A. Mishra and M. Kumar, SN Appl. Sci. **2**, 1 (2020).

[20] G. K. Ramesh, S. Manjunatha, G. S. Roopa, and A. J. Chamkha, J. Therm. Anal. Calorim. 1 (2020).